*Stanford Exploration Project, Report 112, November 11, 2002, pages 83–96*

# Deconvolution imaging condition for reverse-time migration

*Alejandro A. Valenciano and Biondo Biondi*[1]

**ABSTRACT**

The reverse-time migration imaging condition can be improved by computing the reflection strength at each subsurface point as the zero lag value of the deconvolution of the receiver wavefield by the source wavefield. I show that by using this approach it is possible to eliminate image artifacts due to wavefield multipathing through velocity anomalies. I also show that it has the advantage of handling better amplitudes during imaging.

## INTRODUCTION

The most common implementation of shot-profile reverse-time migration (Etgen, 1986; Biondi, 2002) uses the zero lag of the cross-correlation of the source and the receiver wavefields as the imaging condition. This implementation has the advantage of being robust and honoring the kinematics of Claerbout's imaging principle but does not honor the dynamics of the problem, which results in the loss of resolution and amplitude accuracy (Claerbout, 1971).

Another drawback of this imaging condition is that it creates image artifacts when there is a complex propagation pattern, e.g., a low velocity anomaly that cause wavefield multipathing. Let us consider waves propagating in a homogeneous medium with a velocity anomaly and a flat reflector. After the wave traveling directly from the shot to the reflector arrives, a second wave arrives, which has traveled along a different path due to the low velocity anomaly. If the second wave is not accounted for in the imaging process, the single reflector will be imaged as more than one reflector. This could mislead the geological interpretation.

In this paper, we introduce an imaging condition that computes the reflection strength as the zero lag of the deconvolution of the receiver wavefield by the source wavefield. This new process can account for the second wave arrival in the imaging. We implemented two equivalent deconvolution methods: one in the time domain based on least-squares inversion filtering and the other in the Fourier domain.

We illustrate the wavefield deconvolution imaging condition with two different data sets. One created by the convolution of a minimum-phase, band-limited wavelet with a spike series, and the other by wave equation modeling and downward propagation.

[1]**email:** valencia@sep.stanford.edu, biondo@sep.stanford.edu

## REFLECTOR MAPPING IMAGING CONDITION AND IMAGE ARTIFACTS

Claerbout (1971) expresses the reflector mapping imaging condition as follows:

$$\mathbf{r}(x,z) = \frac{\mathbf{u}(x,z,t_d)}{\mathbf{d}(x,z,t_d)}, \tag{1}$$

where $x$ is the horizontal coordinate, $z$ is the depth, and $t_d$ is the time at which the source wavefield $\mathbf{d}(x,z,t_d)$ and the receiver wavefield $\mathbf{u}(x,z,t_d)$ coincide in time and space. This principle states that the reflectivity strength $\mathbf{r}(x,z)$ depends only on the source wavefield and on the receiver wavefield at time $t_d$.

A practical way to compute the reflectivity strength is discussed in Claerbout's paper (Claerbout, 1971). The reflectivity strength is computed as:

$$\mathbf{r}(x,z) = (\mathbf{u} \star \mathbf{d})(x,z,\tau = 0), \tag{2}$$

where $\star$ means cross-correlation and $\tau$ is the lag. This is commonly used in the industry. It has the advantage of being robust, but has the disadvantage of not computing the correct amplitudes (Claerbout, 1971).

A more general imaging condition can be stated, computing the reflectivity strength as:

$$\mathbf{r}(x,z) = \frac{\mathbf{u}}{\mathbf{d}}(x,z,\tau = 0), \tag{3}$$

where the division means deconvolution in time of the receiver wavefield by the source wavefield for each $(x,z)$ and $\tau$ is the lag. It has the potential of accounting for wavefield multipathing during imaging, thus avoiding the creation of image artifacts in the presence of velocity anomalies.

Figures 1 to 3 show the comparison of wavefield deconvolution with wavefield cross-correlation imaging condition. The first row, in Figure 1, simulates the two wavefields coinciding at the reflector depth. The result of the cross-correlation and the result of the deconvolution is shown in the second row. For each case, the zero lag of the wavefield cross-correlation or the zero lag of the wavefield deconvolution is assigned as the reflectivity strength at this depth.

The first row in Figure 2 / 3 simulates the two wavefields at a deeper / shallower depth than the reflector depth. The second row shows the result of the cross-correlation and the result of the deconvolution. The zero lag value of the wavefield cross-correlation has a value different than zero, thus creates an image artifact at a deeper / shallower depth. In the case of deconvolution imaging condition, the zero lag value is zero, thus no image artifacts are created.

The imaging condition stated in equation (3) makes the strong assumption that the receiver wavefield $\mathbf{u}(x,z,t)$ can be computed by convolving the source wavefield $\mathbf{d}(x,z,t)$ by the reflectivity strength $\mathbf{r}(x,z)$. As we will discuss later, this is true at the reflector depth, but might not be true at a different depth.

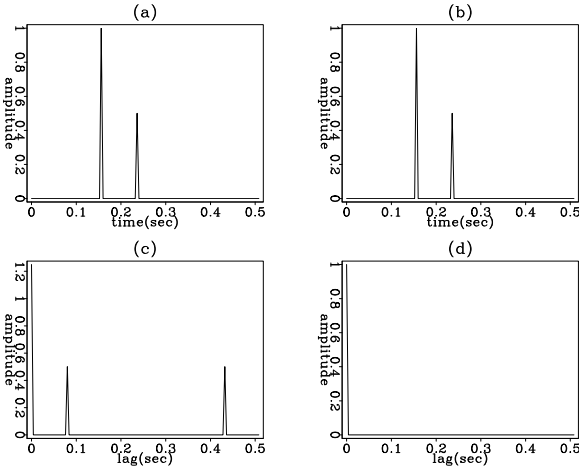


Figure 1: Wavefields coinciding at the reflector depth. (a) Source wavefield. (b) Receiver wavefield. (c) Wavefields cross-correlation. (d) Wavefields deconvolution. alejandro1-spike [ER]

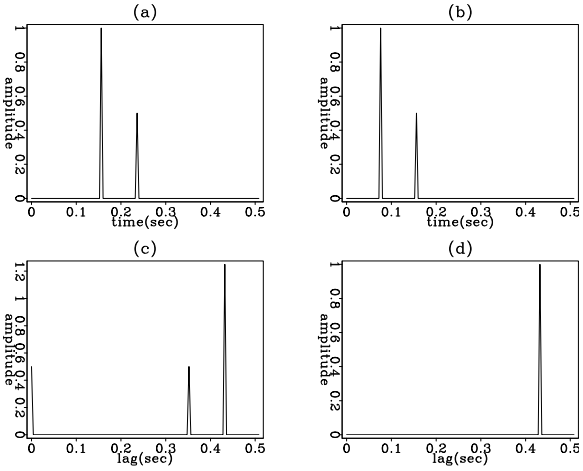


Figure 2: Wavefields at a depth deeper the reflector depth. (a) Source wavefield. (b) Receiver wavefield. (c) Wavefields cross-correlation. (d) Wavefields deconvolution. alejandro1-spike1 [ER]

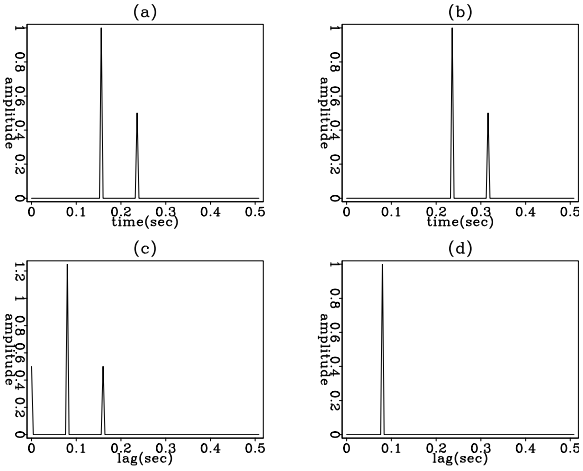


Figure 3: Wavefields at a depth shallower the reflector depth. (a) Source wavefield. (b) Receiver wavefield. (c) Wavefields cross-correlation. (d) Wavefields deconvolution. alejandro1-spike2 [ER]

## DECONVOLUTION IN THE TIME DOMAIN

Deconvolution in the time domain can be implemented in terms of the following fitting goal for each $(x,z)$ location:

$$\mathbf{Dr} = \mathbf{u}, \tag{4}$$

where $\mathbf{D}$ is a convolution matrix whose columns are downshifted versions of the source wavefield $\mathbf{d}$.

The least-squares solution of this problem is

$$\mathbf{r} = (\mathbf{D}'\mathbf{D})^{-1}\mathbf{D}'\mathbf{u}. \tag{5}$$

where $\mathbf{D}'$ is the adjoint of $\mathbf{D}$. A damped solution may be used to guarantee $\mathbf{D}'\mathbf{D}$ to be invertible as in

$$\mathbf{r} = (\mathbf{D}'\mathbf{D} + \varepsilon^2)^{-1}\mathbf{D}'\mathbf{u} \tag{6}$$

where $\varepsilon$ is a small positive number. Equation (6) can be written in terms of the fitting goals

$$\begin{aligned} \mathbf{0} &\approx \mathbf{Dr} - \mathbf{u} \\ \mathbf{0} &\approx \varepsilon\mathbf{Ir}, \end{aligned} \tag{7}$$

where $\mathbf{I}$ is the identity matrix. This approach can be computational efficient if the time window is not too large and we use a Conjugate Gradient as optimization engine. However, it has the disadvantage of relying on a linear inversion process that may or may not converge to the global minimum. A way to overcome this problem, obtaining an analytical solution, is to implement equation (6) in the Fourier domain, as we do in the next section.

## DECONVOLUTION IN THE FOURIER DOMAIN

Jacobs (1982) compares various imaging methods for shot-profile migration. He shows that the deconvolution imaging condition

$$\mathbf{r}(\omega) = \frac{\mathbf{u}(\omega)\bar{\mathbf{d}}(\omega)}{\mathbf{d}(\omega)\bar{\mathbf{d}}(\omega) + \varepsilon^2} \tag{8}$$

is stable. The same imaging condition was used by Lee et al. (1991) in split-step migration.

Since we are only interested in the zero-time lag, the reflection strength can be computed as

$$\mathbf{r}(x,z,\tau=0) = \sum_{\omega}^{\omega_{Nyq}} \mathbf{r}(x,z,\omega). \tag{9}$$

where $\omega_{Nyq}$ is the Nyquist frequency.

An advantage of working in the Fourier domain is that the problem does not need to be stated as an inversion problem.

## DECONVOLUTION IN THE FOURIER DOMAIN WITH BAND-LIMITED DATA

In equation (9) the reflectivity strength is affected by the bandwidth of the data. Let us consider the case where the source and receiver wavefields coincide at the reflector depth and both have a similar frequency content. The best situation we could have is for their division to be a box function. This is unlikely to happen in a real case. Inside the data bandwidth the division is a constant value. But outside of the data bandwidth we may try to divide small numbers by small numbers, which has the potential to be unstable. In equation (8) we use a damping factor to avoid this source of instability but when we apply equation (9) we end up with values that were supposed to be zero contributing to the reflectivity strength.

A different implementation of equation (8), forcing hard zeros when $\mathbf{d}(\omega)\bar{\mathbf{d}}(\omega) < \varepsilon^2$, reduces the impact of band-limited data in the reflectivity strength calculation as

$$\mathbf{r}(\omega) = \begin{cases} \frac{\mathbf{u}(\omega)}{\mathbf{d}(\omega)} & \mathbf{d}(\omega)\bar{\mathbf{d}}(\omega) > \varepsilon^2 \\ 0 & \text{otherwise.} \end{cases} \tag{10}$$

There is another source of error for the band-limited. The Fourier pair of the box function is a sinc function. In the extreme case of a infinite wide box the Fourier pair is a delta function centered at zero lag. As the box is getting narrower in the Fourier domain, the delta becomes a wider sinc function in the time domain. Therefore, the reflectivity strength $\mathbf{r}(x,z,\tau=0)$ is a scaled version of his infinite bandwidth version. We can compensate for the bandwidth of the data by computing the zero lag of the deconvolution as

$$\mathbf{r}(x,z,\tau=0) = \frac{\omega_{Nyq}}{\Delta\omega_{BW}} \sum_{\omega}^{\omega_{Nyq}} \mathbf{r}(x,z,\omega), \tag{11}$$

where $\omega_{Nyq}$ is the Nyquist frequency and $\Delta\omega_{BW}$ is the bandwidth, then zero lag of the deconvolution corresponds to the reflectivity strength. In this case the bandwidth $\Delta\omega_{BW}$ is defined as the frequency range where the inequality $\mathbf{d}(\omega)\bar{\mathbf{d}}(\omega) > \varepsilon^2$ holds.

## TEST WITH SYNTHETIC DATA (CONVOLUTIONAL MODEL)

We tested the different implementations of the imaging condition with synthetic data. The data simulates the case when source and receiver wavefields coincide at reflector depth and the case when they coincide at a shallower depth. The data are constructed by convolving a minimum-phase, $25Hz$ central frequency, band-limited wavelet with a series of spikes.

Figure 4 shows the deconvolution of the signal by itself. The signal was constructed by convolving the wavelet with two spikes. This simulates the situation where source and receiver wavefields coincide at reflector depth. As expected, the result is a delta function centered at zero lag with no difference between the two deconvolution methods (Figures 4d and 4e). Figure 4c shows the result of the cross-correlation for the sake of comparison. The cross-correlation result differs from the deconvolution result in resolution, but still is a symmetric function centered at zero lag.

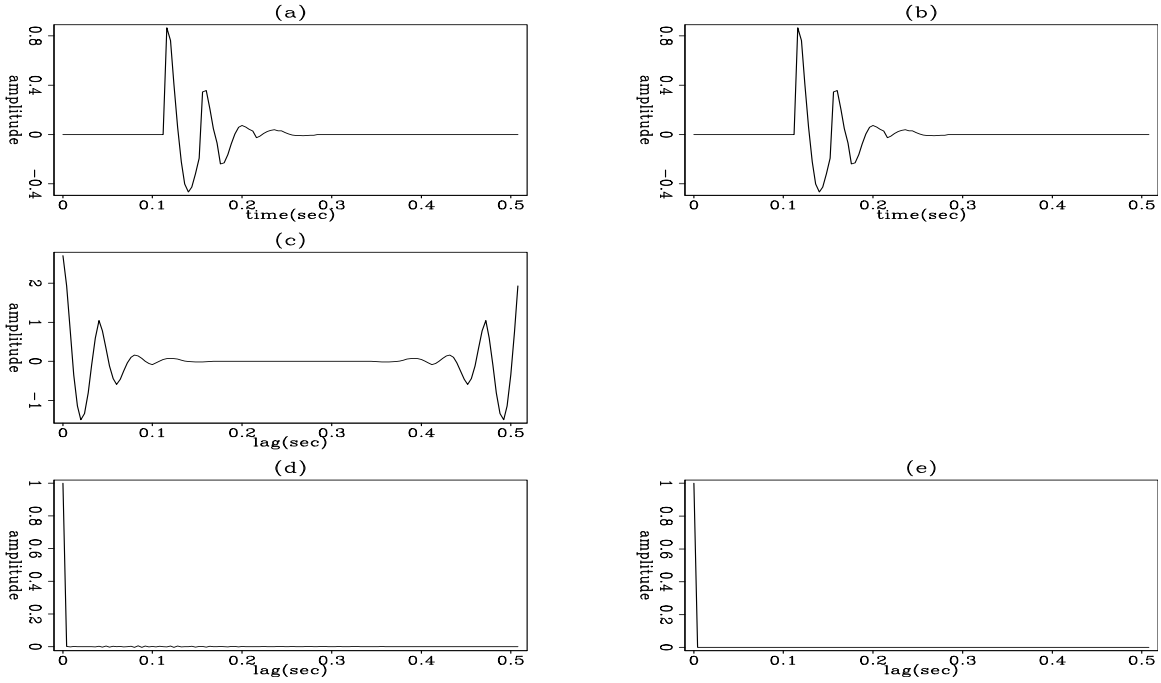


Figure 4: Source and receiver wavefields shifted from zero, simulating wavefields coinciding at the reflector depth. (a) Source wavefield (b) Receiver wavefield (c) Cross-correlation (d) Deconvolution (b) by (a) in the time domain (e) Deconvolution (b) by (a) in the Fourier domain. alejandro1-shift [ER]

Figure 5 shows the result of deconvolving the same signal shifted to the right (Figure 5b) by the unshifted signal (Figure 5a). This simulates the situation where the receiver and the source wavefield coincide at a depth shallower than the reflector depth. The result is a shifted delta function. No significant differences can be seen between the two convolution methods. In this situation the cross-correlation (Figure 5c) produces an erroneous image since the zero lag is different than zero.

Figure 6 shows the deconvolution of the same signal (in Figure 4b) contaminated by more spikes (Figure 6b) with the original signal (Figure 6a). This resembles a real situation when source and receiver wavefields coincide at reflector depth. The deconvolution method based on least squares inversion in time gets the correct value at zero lag but does not converge to the global minimum. In the Fourier domain the delta at zero is recuperated and some energy comes at the end of the signal due to symmetric boundary conditions. Since we are only interested in the zero lag value, both deconvolution methods could be used. The result of the cross-correlation (Figure 6c) has a maximum at zero lag as expected.

Figure 7 shows the deconvolution of the same signal (in Figure 6b) shifted to the right (Figure 7b). This simulates the situation where the receiver and the source wavefield coincide at a depth shallower than the reflector depth. The deconvolution method based on least squares inversion in the time domain recovers the correct shifted spike. As we saw in the previous case, when some energy exist before the onset of the reflector energy in the receiver wavefield,

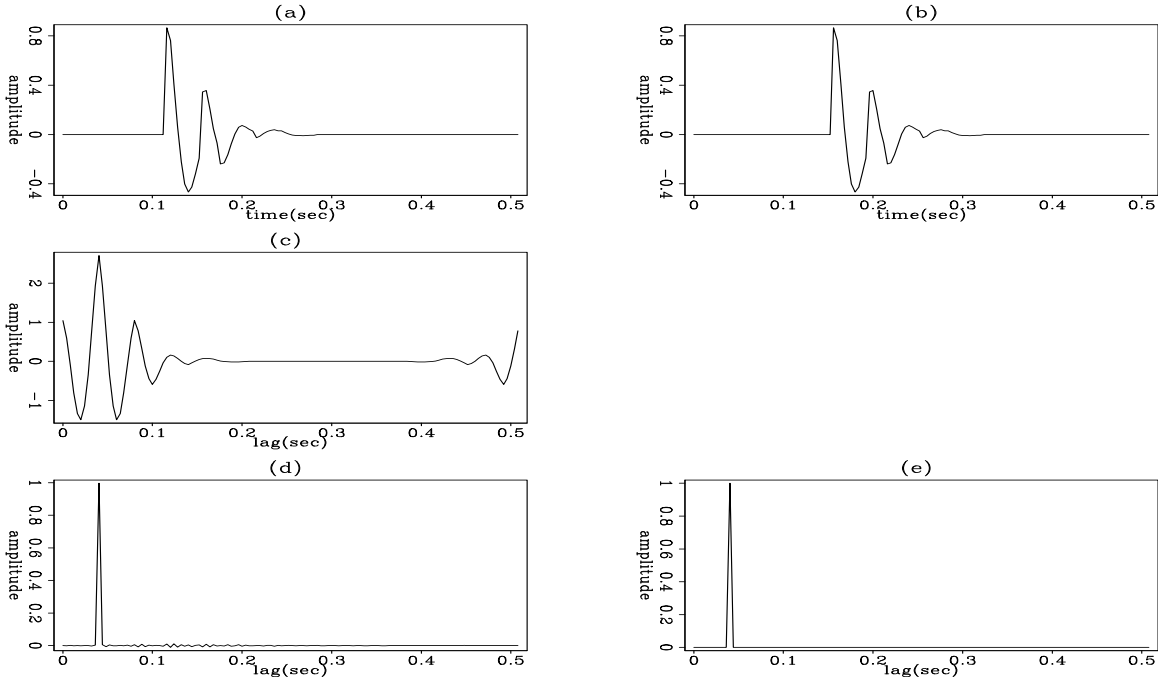


Figure 5: Source and receiver wavefields shifted from zero and each others, simulating wavefields coinciding at a depth shallower the reflector depth. (a) Source wavefield (b) Receiver wavefield (c) Cross-correlation (d) Deconvolution (b) by (a) in the time domain (e) Deconvolution (b) by (a) in the Fourier domain. alejandro1-shift_dt [ER]

the least squares fails to reach the global minimum. In the Fourier domain, we recover the shifted spike and some energy comes at the end of the signal due to symmetric boundary conditions. In this case the deconvolution in the Fourier domain has a better performance than the deconvolution in the time domain since there is no energy at zero lag, as was theoretically predicted.

## TEST WITH SYNTHETIC DATA (WAVE EQUATION)

Now, we test our imaging condition with a more realistic model. The data are modeled with a wave equation-finite differences program. Figure 8 shows the velocity model. Note the low velocity anomaly at 300 m depth. Also, a flat, constant-impedance contrast interface is located at 700 m. The low velocity anomaly creates multipathing that we want to include during the imaging.

From the whole receiver $\mathbf{u}(z,x,t)$ and source $\mathbf{d}(z,x,t)$ wavefields we extracted two constant depth planes: one at the reflector depth (Figure 9) and one shallower (Figure 10). In both figures we can see two reflectors, one due to the direct arrival and the other due to the second wave arrival produced by the low velocity anomaly.

Four traces were extracted for this test at two different offsets (1000 m and 2000 m).

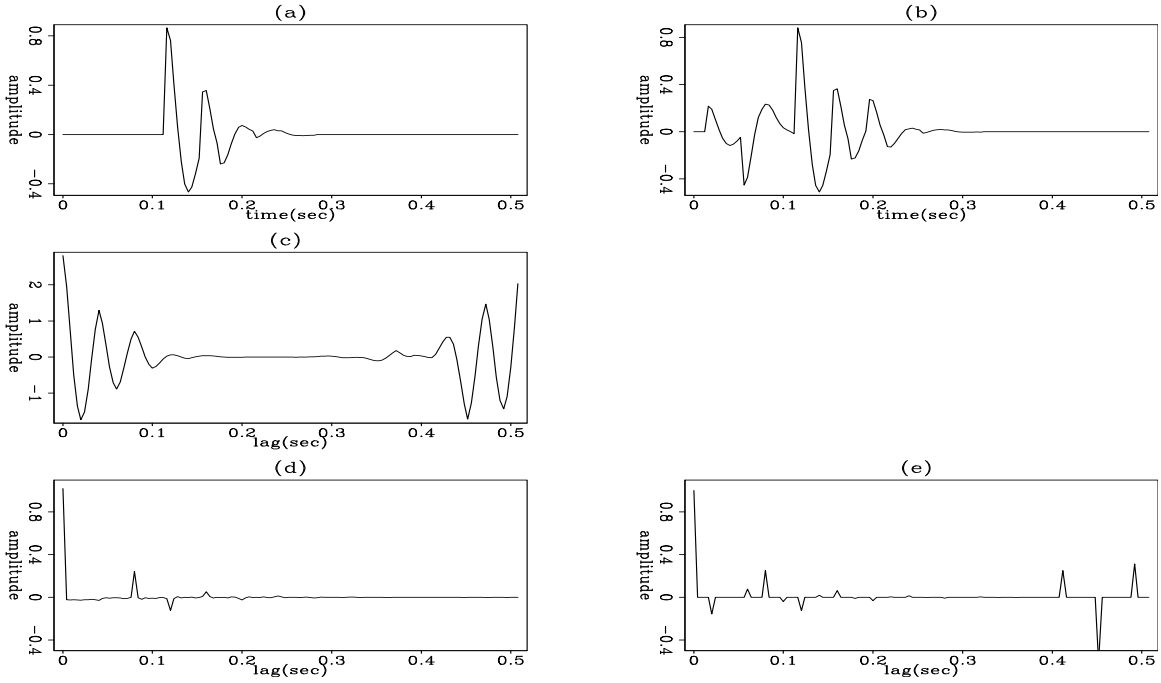


Figure 6: Source and receiver wavefields shifted from zero. It simulates two wavefields coinciding at the reflector depth. Receiver wavefield contaminated with more events. (a) Source wavefield (b) Receiver wavefield (c) Cross-correlation (d) Deconvolution (b) by (a) in the time domain (e) Deconvolution (b) by (a) in the Fourier domain. alejandro1-shift_mult [ER]

Figures 11a and 12a show the source wavefield and Figures 11b and 12b the receiver wavefield at reflector depth. Figures 13a and 14a show the source wavefield and Figures 13b and 14b the receiver wavefield at a shallower depth.

Figures 11 and 12 show the deconvolution of the receiver by the source wavefield at the reflector depth. As we expected, there is a maximum at zero lag. The result is very similar using both deconvolution methods. Convolution of the source wavefield with the reflectivity seems to be a good modeling operator, at least at the reflector depth, since the data residual in the least squares inversion is small.

Figures 13 and 14 show the deconvolution of the receiver by the source wavefield at a depth shallower than the reflector depth. As we expected, the value at zero lag is an order of magnitude smaller than the value at zero lag at the reflector depth. The result is very similar using both deconvolution methods. For an offset of 2000 m and a depth of 500 m, the data residual in the least squares inversion is small, indicating that the convolution of the source wavefield with the reflectivity fits the receiver wavefield. But for an offset of 1000 m and a depth of 500 m, the data residual in the least squares inversion is not small. The explanation for this result can be found looking at Figures 13a and 13b. We can note that the separation between the two arrivals in the source and receiver wavefields is not the same. Thus the source wavefield convolved with a simple delta shifted from the zero lag (as reflectivity) is not enough to explain the receiver wavefield. The impact of this issue in the final image quality

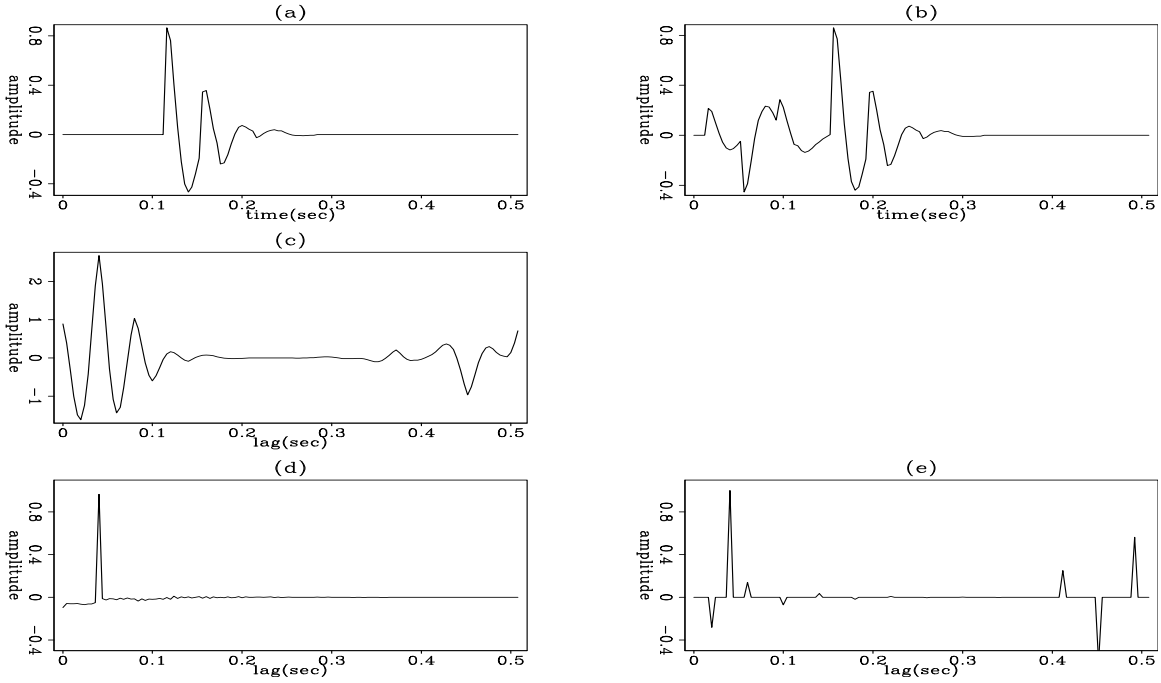


Figure 7: Source and receiver wavefields shifted from zero and each others. It simulates two wavefields coinciding at a depth shallower the reflector depth. Receiver wavefield contaminated with more events. (a) Source wavefield (b) Receiver wavefield (c) Cross-correlation (d) Deconvolution (b) by (a) in the time domain (e) Deconvolution (b) by (a) in the Fourier domain. alejandro1-shift_mult_dt [ER]

needs further investigation.

Comparing the deconvolution with the cross-correlation imaging condition in Figures 11, 12, 13, and 14, we conclude that deconvolution imaging condition effectively attenuates the image artifacts and handles the amplitudes better. In addition, the deconvolution imaging condition does a better job than the cross-correlation in preserving the amplitudes through the offset.

## CONCLUSIONS

The cross-correlation of the receiver wavefield by the source wavefield imaging condition has the advantage of being robust and honoring the kinematics of Claerbout's imaging principle. However, it has the disadvantage of losing resolution and creating image artifacts in the presence of multipathing.

A better imaging condition is obtained by computing the reflection strength as the zero lag value of the deconvolution of the receiver wavefield by the source wavefield. This approach was implemented in the time domain using least squares inverse filters and in the Fourier domain as the scale sum of the frequency components of the wavefields division.

Using the zero lag of the deconvolution imaging condition, we attenuate image artifacts due to wavefield multipathing through velocity anomalies. Also, we showed that it better handles amplitudes during imaging. The preceding statements are corroborated using two different synthetic data sets: one based on the convolutional model and the other based on a wave equation modeling program.

## ACKNOWLEDGMENTS

I would like to thank Morgan Brown for his Fortran 90 programming assistance and Gabriel Alvarez for many discussions about deconvolution.

## REFERENCES

Biondi, B., 2002, Prestack imaging of overturned and prismatic reflections by reverse time migration: SEP–**111**, 123–139.

Claerbout, J. F., 1971, Toward a unified theory of reflector mapping: Geophysics, **36**, no. 3, 467–481.

Etgen, J., 1986, Prestack reverse time migration of shot profiles: SEP–**50**, 151–170.

Jacobs, B., 1982, The prestack migration of profiles: SEP–**34**.

Lee, D., Mason, I. M., and Jackson, G. M., 1991, Split-step fourier shot-record migration with deconvolution imaging:, *in* Geophysics Soc. of Expl. Geophys., 56, 1786–1793.

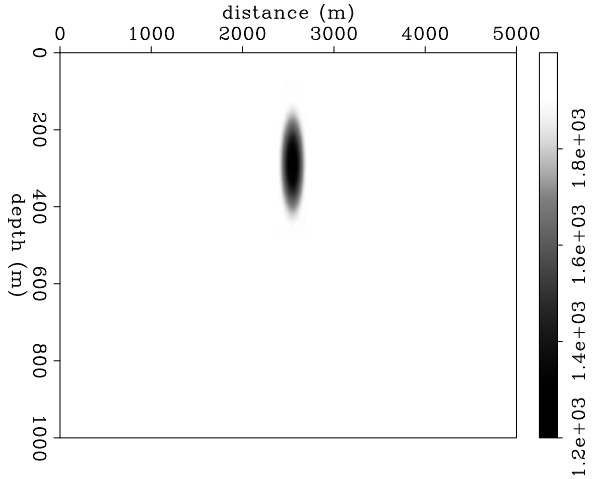


Figure 8: Velocity model with a Gaussian low velocity anomaly. alejandro1-velocity [ER]

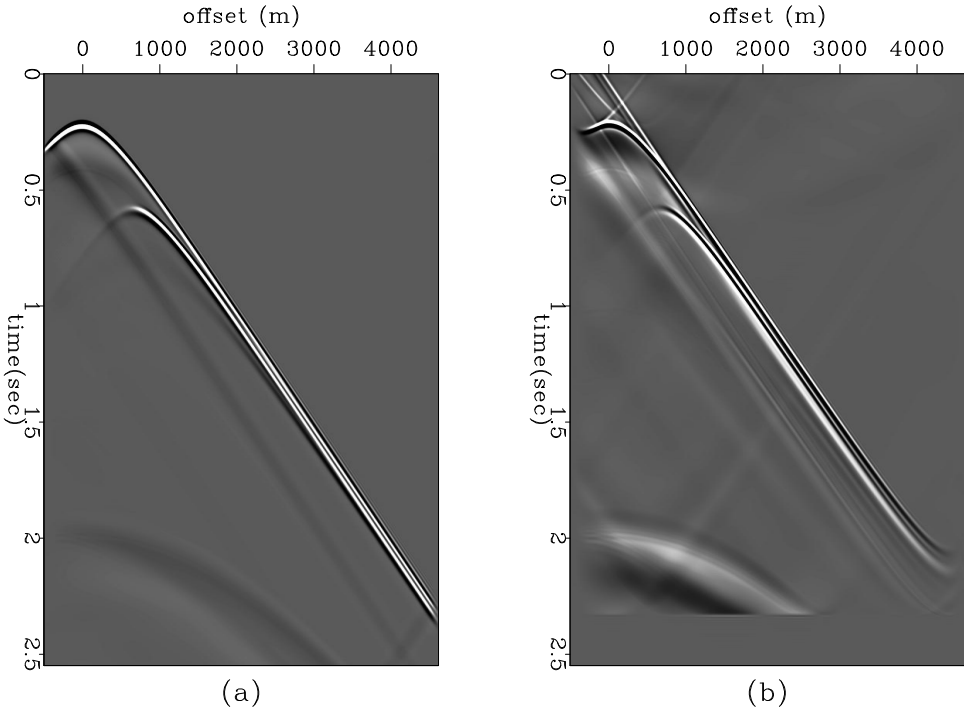


Figure 9: (a) Source wavefield. (b) Receiver wavefield at the reflector depth (700 m). alejandro1-shot-700 [ER]

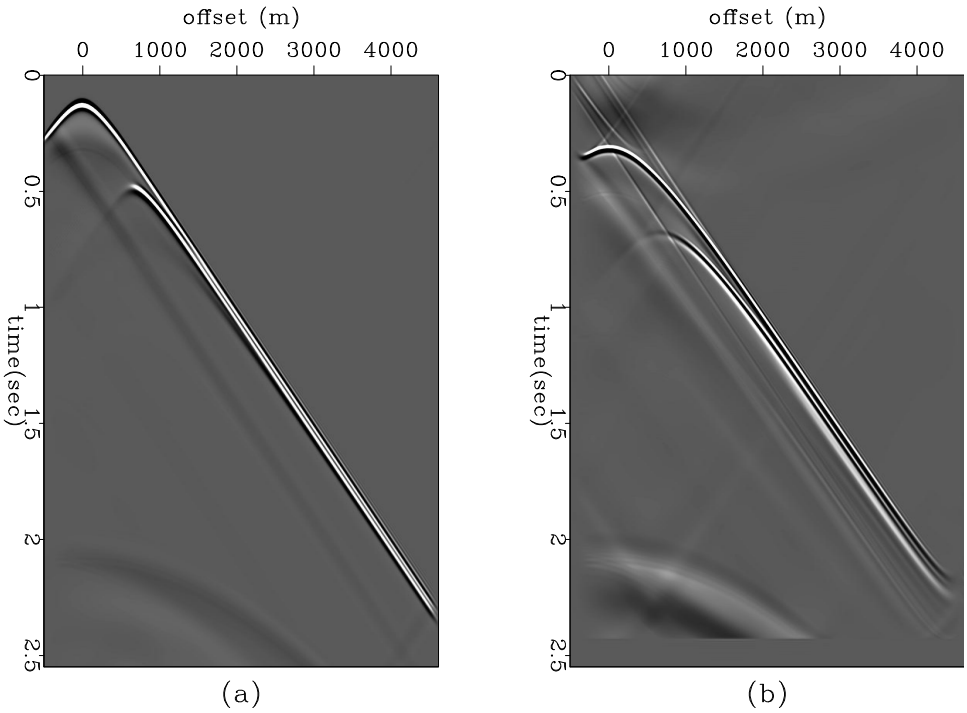


Figure 10: (a) Source wavefield. (b) Receiver wavefield at a shallower depth position (500 m). alejandro1-shot-500 [ER]

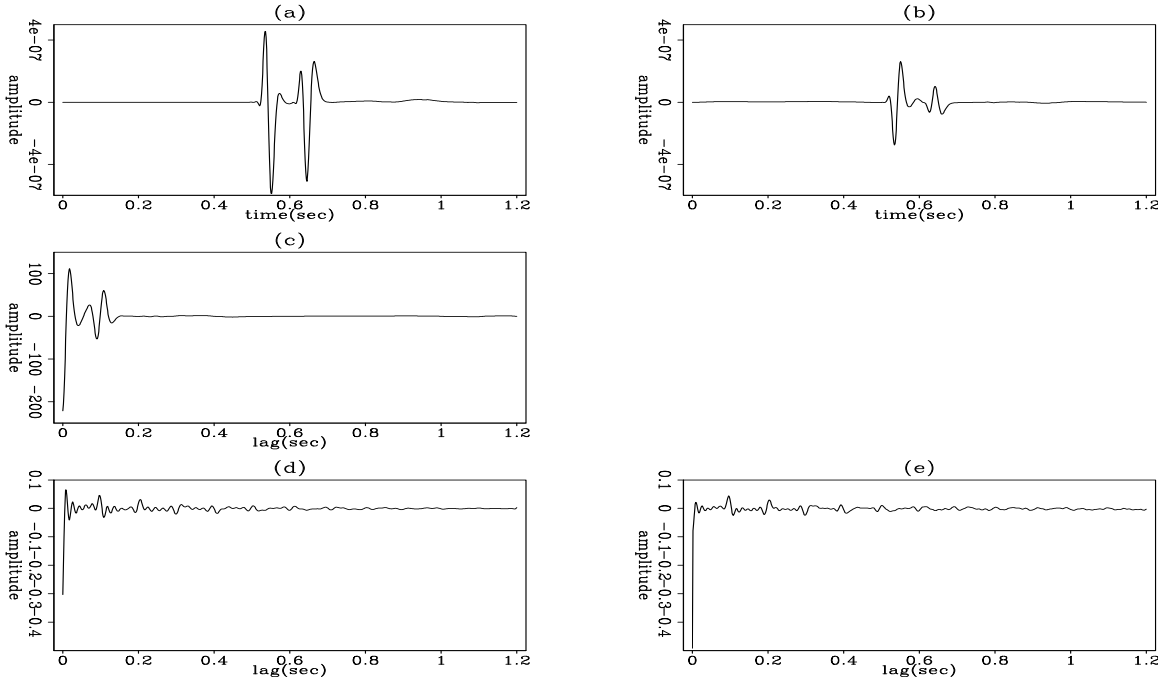


Figure 11: Source and receiver wavefields at the reflector depth at 1000 m offset. (a) Source wavefield (b) Receiver wavefield (c) Cross-correlation (d) Deconvolution (b) by (a) in the time domain (e) Deconvolution (b) by (a) in the Fourier domain. alejandro1-700 [ER]

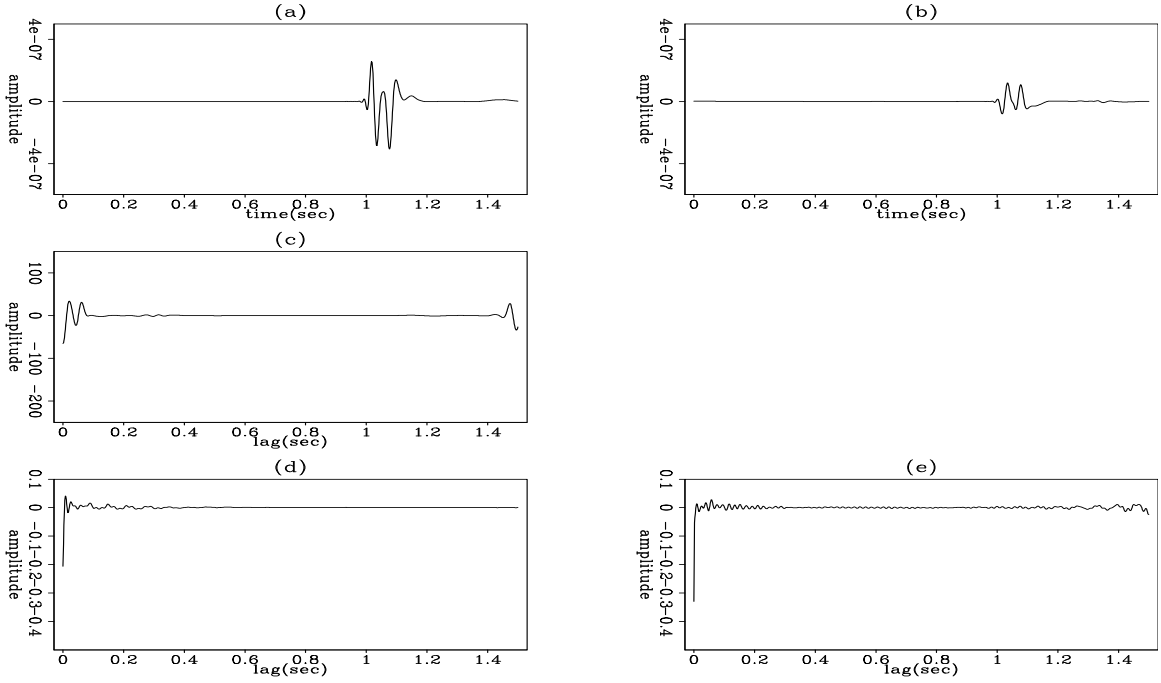


Figure 12: Source and receiver wavefields at the reflector depth at 2000 m offset. (a) Source wavefield (b) Receiver wavefield (c) Cross-correlation (d) Deconvolution (b) by (a) in the time domain (e) Deconvolution (b) by (a) in the Fourier domain. alejandro1-700-2000 [ER]

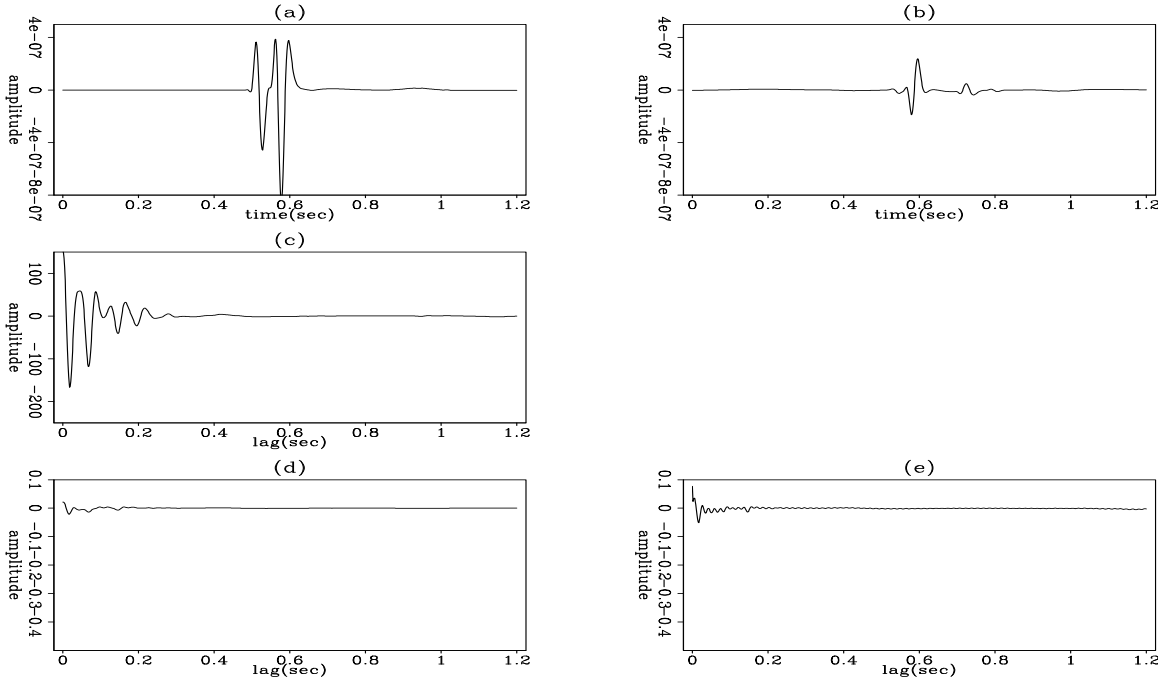


Figure 13: Source and receiver wavefields shallower than the reflector depth at 1000 m offset. (a) Source wavefield (b) Receiver wavefield (c) Cross-correlation (d) Deconvolution (b) by (a) in the time domain (e) Deconvolution (b) by (a) in the Fourier domain. alejandro1-500 [ER]

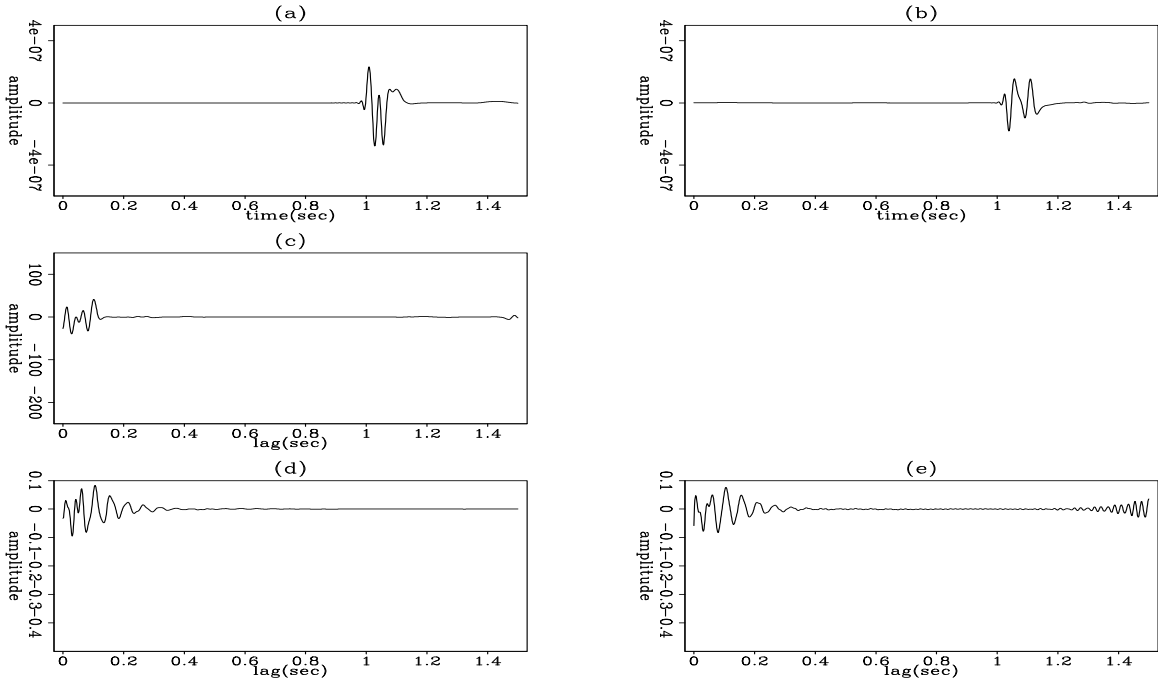


Figure 14: Source and receiver wavefields shallower than the reflector depth at 2000 m offset. (a) Source wavefield (b) Receiver wavefield (c) Cross-correlation (d) Deconvolution (b) by (a) in the time domain (e) Deconvolution (b) by (a) in the Fourier domain. alejandro1-500-2000 [ER]